Analytical Methods

ROYAL SOCIETY OF CHEMISTRY

PAPER

View Article Online
View Journal

Cite this: DOI: 10.1039/d6ay00742b

Real-time resonance Raman spectroscopic monitoring of the Briggs–Rauscher reaction

Clark D. Gray, [a] Nigel Gotts,[a] Cassio Lima, [a] Kenneth Williams,[b] Sebastien Maussang [b] and Royston Goodacre [*a]

The Briggs–Rauscher reaction is a prototypical oscillating system and is based on chemical mixtures of iodate (IO_3^-), hydrogen peroxide, malonic acid and Mn^{2+} ions in an acidic solution. Although the Briggs–Rauscher oscillatory behaviour can be seen visibly, conventional analytical methods lack molecular detail of the exact chemical reactions within this highly dynamic system. Using real-time resonance Raman spectroscopy at 785 nm excitation, we track iodine speciation through distinct triiodide and pentaiodide signatures. Fourier-transform analysis of these time-series Raman data reveals that increasing temperature accelerates oscillation frequency while destabilising oscillatory regularity at elevated temperatures (43 °C); higher iodate concentrations promote regular oscillations at intermediate levels but suppress them through excessive oxidation at high concentrations; and starch actively modulates the reaction by stabilising polyiodide formation and doubling the oscillation period relative to starch-free conditions. This study demonstrates Raman spectroscopy as a precise physicochemical tool for analysing chemical oscillations.

Received 20th April 2026
Accepted 27th May 2026

DOI: 10.1039/d6ay00742b

rsc.li/methods

Introduction

The Briggs–Rauscher (BR) reaction is one of the most significant introductions to demonstrate kinetics within chemical reactions. As it is also part of a larger family of oscillating chemical reactions (OCRs),[1] its behaviour may display non-linear chemistry which has been relatively understudied in real-time monitoring systems. Its oscillatory behaviour is attributed to the mixture of iodate (IO_3^-), hydrogen peroxide, malonic acid and Mn^{2+} ions in an acidic solution (typically pH < 2). The initial solution is colourless before turning amber as iodine (I_2) forms, I_2 binds with starch giving a striking blue-black colour, which then fades to colourless as I_2 is reduced back to iodide (I^-) in a recurring cycle. The reaction oscillates several times before stabilising as a dark blue polyiodide solution (see Fig. 1).

These changes are driven by a series of redox and reduction reactions. Initially, IO_3^- is oxidised to produce molecular iodine using manganese ions ($MnSO_4$) as the metal catalyst:

$$2IO_3^- + 5H_2O_2 + 2H^+ \xrightarrow{Mn^{2+}} I_2 + 5O_2 + 6H_2O \quad (1)$$

I_2 is reduced to I^- by malonic acid:

$$2I_2 + 5CH_2(COOH)_2 + IO_3^- + H^+ \rightarrow 5CHI(COOH)_2 + 3H_2O \quad (2)$$

IO_3^- is further used in the autocatalytic formation of I_2, which forms with starch to generate the striking blue colour.

In this reaction, the excess I_2 binds to I^- ions in a reversible reaction, forming different polyiodide species. Of these, triiodide (I_3^-) and pentaiodide (I_5^-) are well-established in aqueous solution and are the species most readily detectable by Raman spectroscopy under the conditions of this study.[2,3] Higher-order polyiodides such as I_4^{2-}, I_6^{2-}, I_7^-, and I_8^{2-} have been characterised primarily in the solid state or in highly concentrated iodide solutions, and their occurrence in dilute aqueous reaction mixtures under BR conditions is not well established.[4]

Monitoring these reactions relies on both visual recordings and potentiometer probes, with a strong preference for using a ion-selective electrode[5] and less of an emphasis on monitoring the chemical constituents, particularly for fast oscillations where it is currently not possible to quench the reaction so that time consuming chemical analyses can be conducted. In reality, there is an incomplete set of 30 postulated intermediary and sub-elementary processes that induce the oscillation of the BR reaction, some of which have had their reaction coefficients established *via* computational modelling.[6,7]

Iodide-selective probes are the most widely used in monitoring the BR reaction.[8,9] A key limitation of these probes is their poor specificity: rather than measuring a single species, the recorded potential shifts between different potential-

[a]*Centre for Metabolomics Research, Department of Biochemistry, Cell and Systems Biology, Institute of Systems, Molecular and Integrative Biology, University of Liverpool, BioSciences Building, Crown St., Liverpool L69 7ZB, UK. E-mail: roy.goodacre@liverpool.ac.uk*

[b]*Renishaw plc, Spectroscopy Products Division, New Mills, Kingswood, Wotton-under-Edge GL12 8JR, UK*

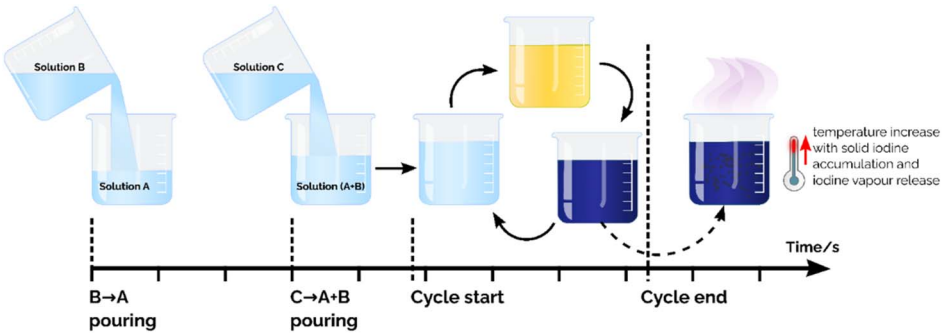

Fig. 1 Distinct reaction phases in the BR reaction, highlighting the cyclical colour evolution of the BR reaction from colourless through amber and blue-black the end of the cycle and the subsequent increase in temperature, iodine vapour release and the precipitation of solid iodine residue.

determining species throughout the oscillation cycle, as the probe responds to other anionic contaminants and multiple interconverting iodine species.[10] Further drawbacks include the need for regular maintenance and calibration,[11] low response sensitivity,[12] and susceptibility to fouling—the accumulation of waste residue on the electrode surface can interfere with measurements.[13]

While UV-visible spectroscopy has also been employed,[14,15] in which the direct molecular modes have been probed over-time, broad bands, overlapping absorbance spectra, and long integration times with low signal-to-noise ratio can complicate interpretation of which chemical components are present and changing during fast oscillatory reactions. There is therefore a need to be able to measure reaction dynamics *in situ* in a non-invasive and non-destructive manner.

The study most directly comparable to the present work is that of Chowdhry *et al.*,[16] who employed kinetic resonance Raman spectroscopy at 632.8 nm excitation to monitor the 160 cm^{-1} pentaiodide band during BR oscillations at different temperatures, demonstrating that oscillation frequency increases with temperature. The present study extends this work in several important respects: (i) a 785 nm excitation laser is employed, which operates further from the $\lambda_{max} = 620$ nm of the starch–iodine complex [17–19] and reduces Franck–Condon enhancement, whereby pre-resonance can simultaneous detect both I_3^- and I_5^- as well as additional reagent bands (IO_3^- at 802 cm^{-1}, H_2O_2 at 877 cm^{-1}, and $MnSO_4$ at 980 cm^{-1}) in the 700–1000 cm^{-1} region; (ii) Hue-Saturation-Value (HSV) video analysis is synchronised with Raman acquisition to provide simultaneous visual and molecular-level information; (iii) the effects of iodate concentration, malonic acid concentration, hydrogen peroxide concentration, and starch presence are systematically investigated; and (iv) DCLS decomposition combined with Fast Fourier Transform (FFT) analysis is used to extract quantitative oscillation frequencies from the Raman time series. DCLS (Direct Classical Least Squares) decomposes each measured spectrum as a weighted linear combination of reference spectra (in this case, the initial mixed solution spectrum and the final polyiodide-rich product spectrum), and the coefficient (score) assigned to each reference spectrum reflects its relative contribution to the measured spectrum at that time point. These scores are dimensionless and were extracted at each 0.5 s acquisition interval; oscillation amplitude was assessed as the peak-to-trough difference in DCLS score within each cycle. In the visual representation, Hue encodes the dominant wavelength of colour on a circular scale (0–360°, where 0°/360° corresponds to red, ~120° to green, and ~240° to blue), saturation describes the intensity or purity of that colour, and value represents overall luminosity. For monitoring the BR reaction, the Hue channel is particularly informative because it is sensitive to the qualitative colour shifts (colourless → amber → blue-black) that accompany changes in iodine speciation, while being relatively insensitive to changes in illumination intensity.

Materials

Solution preparation

All solutions (Thermo Scientific Chemicals, 1 Ashley Road, Altrincham, Cheshire, UK) were prepared using deionised water (1 L). Solution A (pH 1.3 ± 0.1) consisted of potassium iodate (43 g, 200 mM), sulfuric acid (4.5 mL, 45 mM). Solution B (pH 1.8 ± 0.1) contained malonic acid (15.6 g, 150 mM), manganese sulfate monohydrate (3.04 g, 20 mM) and soluble starch (0.4 g, 220 mM). Solution C (pH 2.5 ± 0.1) consisted of hydrogen peroxide (350 mL, 3.08 M). The pH was confirmed using a calibrated pH meter (three-point calibration with NIST-traceable buffers at pH 4.0, 7.0, and 10.0).

Experimental conditions for various concentrations and temperatures

For kinetic investigations, concentrations of potassium iodate (47, 70, 94, 200 mM), malonic acid (0.1, 0.15, 0.2, 0.25 M), and hydrogen peroxide (0.44, 0.88, 1.76, 3.08 M) were varied to assess concentration-dependent impacts on reaction dynamics. These concentrations were chosen because they span a sufficiently broad range to observe measurable changes in oscillation frequency and induction period while remaining within experimentally practical and literature-supported limits that sustain oscillatory behaviour.[20] The influence of temperature was studied by cooling the solutions with dry ice and allowing

equilibration at 5, 13, 17 °C, and then heating the solutions to 22, 29 and 43 °C; these temperature were chosen because they cover a controlled range below and above room temperature, enabling evaluation of temperature dependence and its effect on oscillation rate and stability. Overall, we visibly observed that the mixed solutions oscillated in colour and hue before stabilising to a dark blue (Fig. S2).

Raman analysis of single cycle

Spectroscopic and imaging analysis

Visible video data were acquired using a camera (Sony Device Technology Co. Ltd, Mueang Pathum Thani, Thailand) equipped with a 55 mm focal lens, recording at 30 fps; average luminosity data was extracted from the HSV of each frame from a specified pixel area (252 × 231).Raman spectra were collected every 0.5 s using a Renishaw Virsa™ Raman Analyser (Renishaw plc., Wotton-under-Edge, UK) equipped with a 785 nm laser providing 86 mW power on the sample). Data were collected across 100–1100 cm^{-1} with a 1500/mm grating and a spectral resolution of 1.17 ± 0.14 cm^{-1}. A standoff Raman probe (Renishaw plc.) was positioned using an incremental translation stage to minimise the background exhibited from the glass beaker and to maximise the 802 cm^{-1} band of potassium iodate of Solution A. Solution A (200 mL) and Solution B (200 mL) were placed in a glass beaker, and Solution C (200 mL) was rapidly introduced while simultaneously recording both video and Raman data (see Fig. 2).

Spectral analysis employed Renishaw's WiRE™ software package allowing DCLS to be performed, using the initial spectrum post-mixing as an intermediary reference and the final spectrum as the product. DCLS data were further smoothed using a Weighted Moving Average (WMA) with a bin-span of 3 (equivalent to 1.22 s, see SI for details on Python scripts). The Raman spectra of each individual solution and their sequential mixtures are presented in Fig. S1, providing the spectral reference framework for the DCLS decomposition applied throughout this study; mode assignments are summarised in Table S1. Solution A (potassium iodate in sulfuric acid) is dominated by a sharp, intense band at 802 cm^{-1}, assigned to the symmetric stretching mode (ν_1) of the IO_3^- ion,[21] which serves as the primary spectral marker for iodate throughout the reaction. Additional bands at 980 and 1050 cm^{-1} are attributable to the symmetric and asymmetric modes of SO_4^{-2} introduced by sulfuric acid.[22,23] Solution B (malonic acid, manganese sulfate monohydrate, and starch) displays a more complex spectral profile, with bands at 422, 773, 919, and 980 cm^{-1}. The bands at 919 cm^{-1} and 773 cm^{-1} are consistent C–C chain vibrations and O=C–O deformation of malonic acid,[22] respectively, while the 422 cm^{-1} corresponds to an ion pair HSO_4^- vibration.[24] The band at 980 cm^{-1} reflects the symmetric SO_4^{2-} stretching mode of manganese sulfate monohydrate. No strong starch-specific Raman features were observed under 785 nm excitation, consistent with the relatively weak Raman scattering intensity of amylose-rich starch systems at near-infrared wavelengths.[25] The combined spectrum of Solutions A and B prior to addition of Solution C confirms that no spontaneous reaction occurs between these components and that their individual spectral features are preserved in the mixture.

Solution C (aqueous hydrogen peroxide) is characterised by a prominent band at 877 cm^{-1}, assigned to the O–O stretching mode of H_2O_2,[26] which provides a direct monitor of peroxide concentration throughout the reaction. Upon addition of Solution C to the A + B mixture, the 877 cm^{-1} H_2O_2 band is clearly resolved in the combined intermediary spectrum alongside the 802 cm^{-1} IO_3^- band, confirming that all reagents are spectrally distinguishable at the onset of the reaction.

The spectrum recorded at the end of the reaction (after oscillations have ceased and the solution has stabilised to

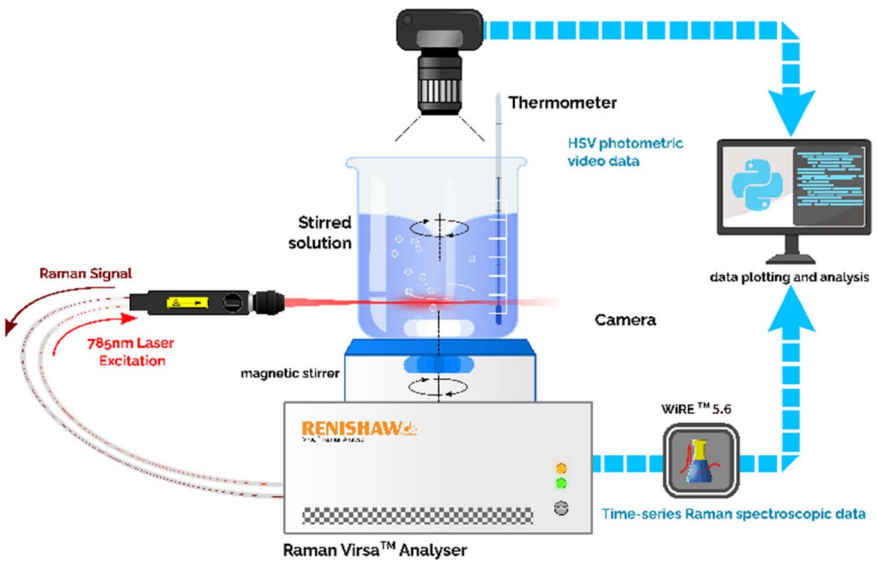

Fig. 2 Camera and stand-off Raman probe setup and data analysis process.

a dark blue colour) shows the emergence of new, intense bands in the low-wavenumber region: at 110 cm^{-1} (triiodide, I_3^-) and 160 cm^{-1} (pentaiodide, I_5^-).

Once the BR reaction has ended, malonic acid is fully consumed and can no longer reduce I_2 into active I^- ions. This results in the takeover of the oxidation reaction, resulting in the build-up of I_2 and its precipitation of solid I_2. Bands at 180 and 189 cm^{-1} correspond to the in-phase and out-of-phase stretching modes of crystalline iodine, respectively.[27] The simultaneous appearance of these solid I_2 modes indicates that, once malonic acid is fully consumed and can no longer reduce I_2 to I^-, molecular iodine precipitates from solution. This is also evident with the increase in temperature by ~5 °C by the oxidation of I^-species to I_2, releasing heat in an exothermic reaction. The elapsed spectrum, accumulated after the reaction has reached its maximum polyiodide content, shows these low-wavenumber bands at full intensity, with a marked decrease in the 802 cm^{-1} IO_3^- band, confirming near-total consumption of iodate. These reference spectra — particularly the initial A + B + C mixture spectrum and the final polyiodide-rich end spectrum—serve as the two end-member components in the DCLS analysis applied to the oscillatory time series, enabling the relative spectral contribution of polyiodide species to be tracked quantitatively as a function of time (Fig. 4a). The term 'spectral contribution' refers to the DCLS score assigned to each reference spectrum component at each time point.

An initial analysis was carried out on the first oscillatory cycle of the BR reaction. Fig. 3a presents the colour evolution extracted from the camera recordings (b) together with the associated spectroscopic data. In aqueous solutions, when I_2 interacts with excess I^- ions, polyiodides such as pentaiodide (I_5^-) and triiodide (I_3^-) are produced. A higher level of enhanced Raman scattering was observed for I_5^- than for I_3^-. Pentaiodides are longer and have weaker bonds compared to triiodides; with a delocalised electronic structure, resulting in greater polarizability changes. These results are consistent with Zhang *et al.*[28]

Full cycle analysis

For this specific configuration, each cycle has a period of approximately 21 s, depending on the temperature, pH, chemical composition. The period of the oscillation also increases over time towards the end of the reaction as the chemical components that sustain the oscillation run out (see Fig. 4). Fig. 4a presents the time-matched correlation between the DCLS-derived polyiodide spectral contribution and the Hue and value extracted from the camera recordings over the full course of the BR reaction. Both traces display periodic oscillations corresponding to successive reaction cycles.

Once the solutions are mixed, the reaction mixture undergoes a rapid colour transition: it changes from colourless to yellow, and then quickly shifts to a deep blue/black within approximately 0.8 s. In contrast, the dominant changes in the spectroscopic signal (DCLS) require around 3.3 s to reach their maximum intensity. A consistent temporal offset is also apparent between the two signals: the Hue channel registers a colour change approximately 2.5 s before the DCLS signal reaches its peak, reflecting the fact that the starch–iodine chromophore is visually detectable at very low polyiodide concentrations, whereas the DCLS signal requires measurable accumulation of I_3^- and I_5^- to register a significant spectral contribution.

This difference in timing indicates that the appearance of the blue starch–iodine colour occurs before the full chemical accumulation of the relevant iodine species. The early blue colour reflects the initial formation of I^- and its interaction with I_2 to produce the starch–polyiodide complex, which is highly chromatic even at low concentrations. However, the formation of larger amounts of polyiodides requires both accumulated I_2 and an excess of I^-, a process that proceeds more slowly. As a result, the DCLS signal continues to rise after the visible colour has already appeared. The progressive increase in cycle period visible in both traces towards the end of the reaction reflects the depletion of reagents, most notably IO_3^- and malonic acid, which sustain the autocatalytic feedback loop.

A gradual baseline rise is apparent in the DCLS time series over the course of the reaction. This is attributable to the progressive accumulation of coloured species (I_2 and polyiodides) in solution, which increases the broad-band fluorescence background and alters the overall spectral baseline. Increasing turbidity as the reaction approaches termination (due to solid I_2 precipitation) also contributes to baseline elevation through enhanced scattering.

Varying environmental conditions

The video recording and the *in situ* Raman acquisition were synchronised by manually temporal aligning the two datasets. To achieve this, we identified distinctive features that appeared in both measurements: (i) small, rapid changes in the value channel (V) of the camera data, and (ii) the first observable intermediate spectral change in the DCLS Raman trace by the addition of Solution C. These features were used as shared temporal markers, allowing the two datasets to be matched to within ±0.5 s. The moment at which Solution C was rapidly poured into the mixture was then assigned a reference time of 30 s. Experimental results from varying malonic acid (Fig. S4), potassium iodate (Fig. S5), hydrogen peroxide (Fig. S6 and S7), and from the absence of starch (Fig. S8) can be found in the SI.

To determine the oscillation frequency of the BR reaction, the DCLS Raman time-series was subjected to a Fast Fourier Transform (FFT), and the dominant peak(s) in the resulting frequency spectrum were taken as the characteristic oscillation frequencies.

Investigating temperature effects

Fig. 5 presents the temperature-dependent DCLS time series (a) and corresponding FFT spectra (b) for temperatures ranging from 5 °C to 43 °C. The FFT converts the periodic DCLS oscillation from the time domain into the frequency domain; the dominant peak in each FFT spectrum corresponds to the fundamental oscillation frequency of the BR reaction at that temperature, expressed in ms^{-1} (cycles per millisecond). A shift

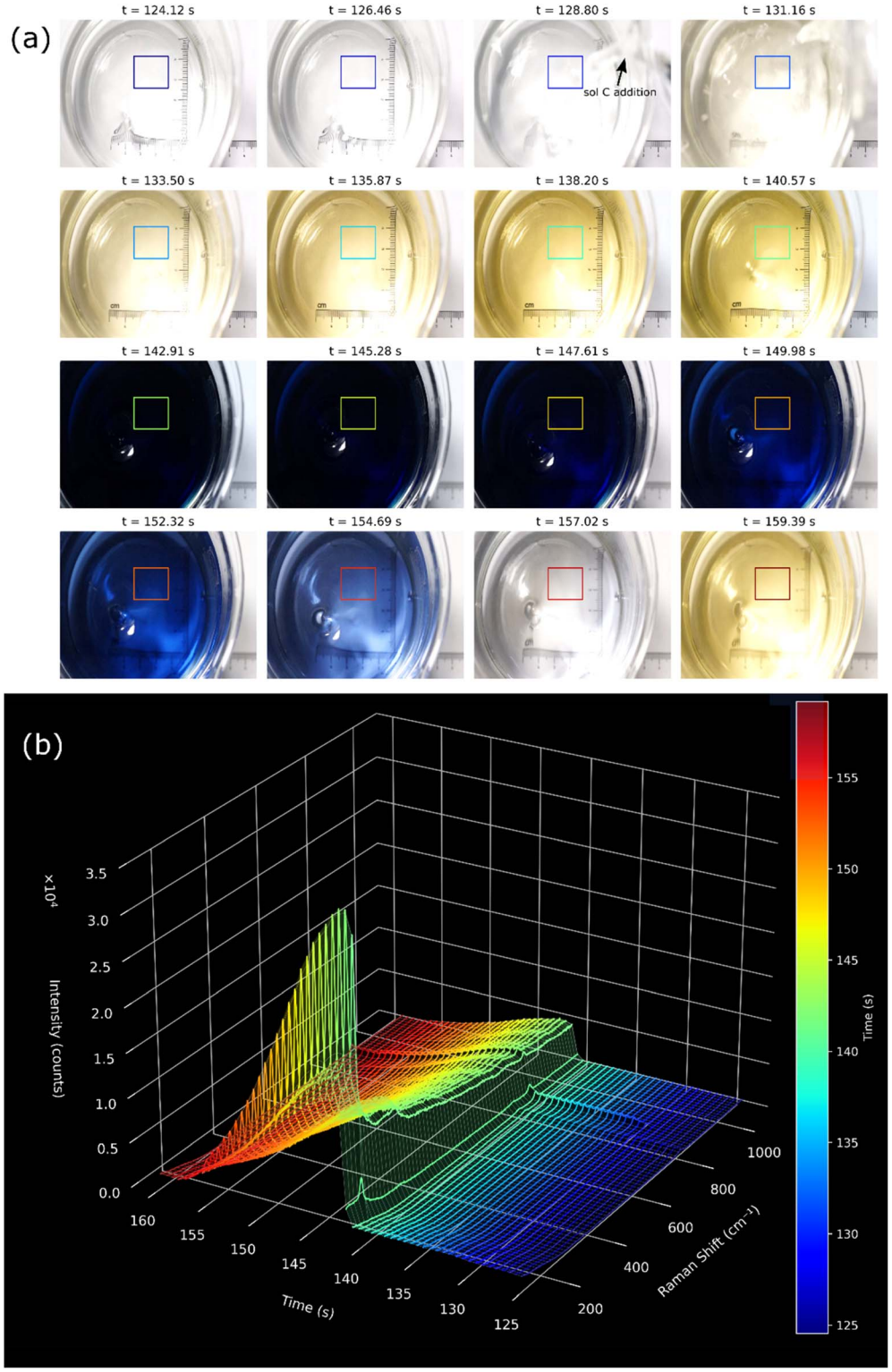

Fig. 3 A single Briggs–Rauscher cycle following the addition of solution C. (a) 16 evenly time spaced camera frames, with the boxed region indicating the pixel area used for HSV-luminosity analysis. (b) Time-series *in situ* Raman spectra showing the transition from solutions A + B through the addition of solution C to the subsequent rapid polyiodide formation.

of this peak to higher frequencies with increasing temperature directly reflects a shortening of the oscillation period.

At lower temperatures (5–13 °C), the FFT reveals a set of single, narrow and dominant frequency peaks, indicating regular, well-defined oscillations. As temperature increases toward 22–29 °C, the dominant frequency increases and additional harmonic content becomes apparent. At 43 °C, the DCLS time series adopts a markedly different profile compared with

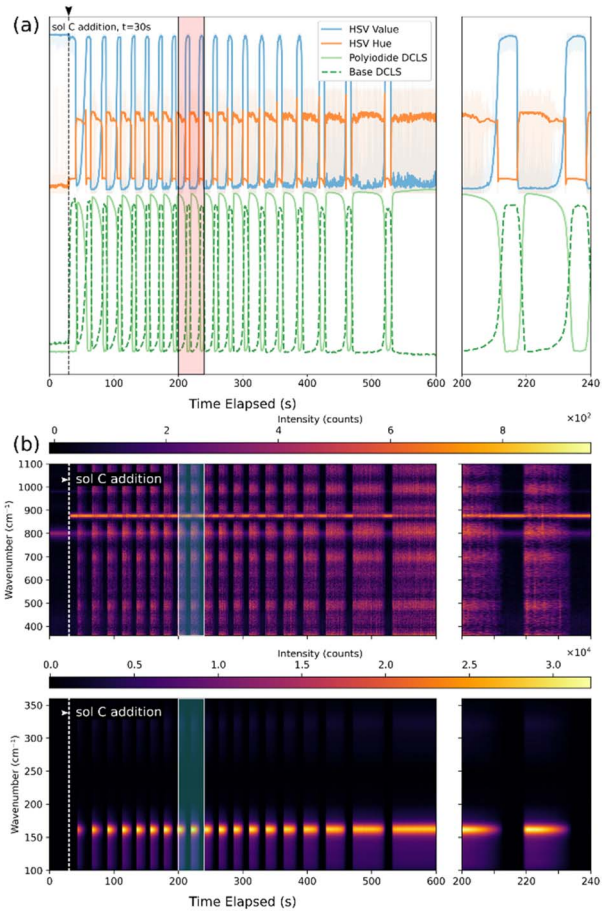

Fig. 4 Time-matched BR reaction data. (a) Correlation between the DCLS-derived polyiodide spectral contribution (left *y*-axis; dimensionless DCLS score representing the relative spectral weight of the polyiodide reference spectrum, primarily reflecting I_3^- and I_5^- contributions in the 100–200 cm^{-1} region) and the HSV Hue value extracted from camera frames (right *y*-axis; Hue in degrees, 0–360°, where increasing Hue toward ~240° reflects the blue-black colour of the starch–polyiodide complex). (b) Corresponding time-matched *in situ* Raman spectroscopic time series showing the full spectral evolution of the BR reaction.

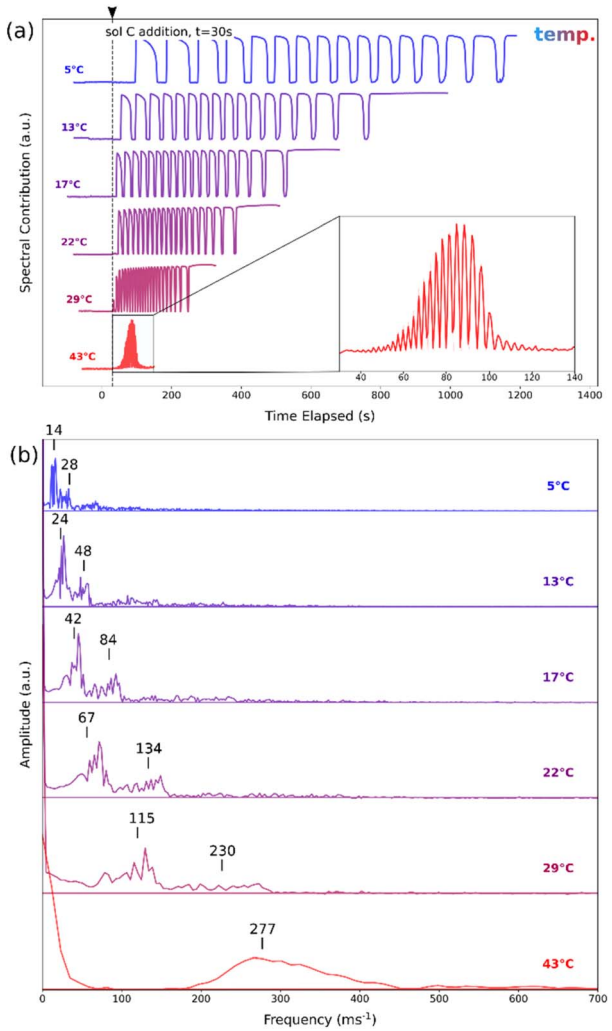

Fig. 5 Temperature-dependent DCLS spectral contributions following the addition of solution C at (t = 30 s). (a) Time-resolved DCLS signals showing increasingly rapid and damped oscillatory behaviour with increasing temperature, culminating in suppression of sustained oscillations at (43 °C). (b) Corresponding FFT spectra showing a systematic shift toward higher frequencies and broader spectral features with increasing temperature.

lower temperatures: rather than displaying well-resolved symmetric oscillations, the trace exhibits a compressed, irregular pattern in which successive peaks are poorly separated, and the reaction rapidly transitions to a terminal state. This behaviour indicates that at 43 °C the accelerated reaction kinetics cause reagent depletion to occur on a timescale comparable to the oscillation period itself, destabilising the autocatalytic feedback loop and disrupting regular oscillatory behaviour. The corresponding FFT at 43 °C consequently shows a broadened, less well-defined frequency peak, consistent with the loss of oscillatory regularity. These observations extend the findings of Chowdhry *et al.*[16] who monitored the 160 cm^{-1} pentaiodide band at 632.8 nm excitation over a narrower temperature range, by providing additional mechanistic detail across a wider temperature window and revealing the onset of dynamical instability at elevated temperatures.

Investigating potassium iodate variation effects

Potassium iodate (KIO_3) provides the IO_3^- ions necessary for the oxidation of IO_3^- to I_2. KIO_3 is also involved in the production of free radical iodine dioxide ($IO_2^\bullet$) from the production of iodous acid (HIO_2) which drives multiple oscillatory reactions:[4,6]

$$IO_3^- + 2H^+ + I^- \leftrightharpoons HOI + HIO_2 \quad (3)$$

$$IO_3^- + 4HIO_2 + H^+ \leftrightharpoons 2IO_2^\bullet + 4H_2O \quad (4)$$

$IO_2^\bullet$ then oxidises manganese(II) (Mn^{2+}) to form hydroxy manganese ($Mn(OH)^{2+}$) and additional HIO_2 to act as an intermediary in the redox cycles:

$$IO_2^\bullet + Mn^{2+} + H_2O \rightarrow HIO_2 + Mn(OH)^{2+} \quad (5)$$

The concentration of IO_3^- is too low at 47 mM, there is insufficient I^- to sustain the autocatalytic feedback loop, triggering no observable reaction (see Fig. S5). Short and fast oscillations are observed at 70 mM: attributed to IO_3^- quickly depleting I^-, generating rapid fluctuations in I^-. With the addition of more KIO_3, higher concentrations of IO_3^- can stabilise regular oscillations. With ever higher concentrations of IO_3^- (200 mM), the fast oscillations quickly slow down and disappear due to excessive oxidation. Higher concentrations of KIO_3 still leads to slower oscillations, seen in the decreasing dominant frequencies.

Investigating the role of starch in the BR reaction

Starch has been largely added in the BR reaction as colouring indicator—conventionally used in a passive role—to display the presence of I_2 since I_2 complexes with its hydrophobic helical structures. Upon examining a BR reaction without starch, it was found that the presence of starch can significantly influence the reaction dynamics. Each reaction—starch and non-starch reactions—were analysed at 22 °C.

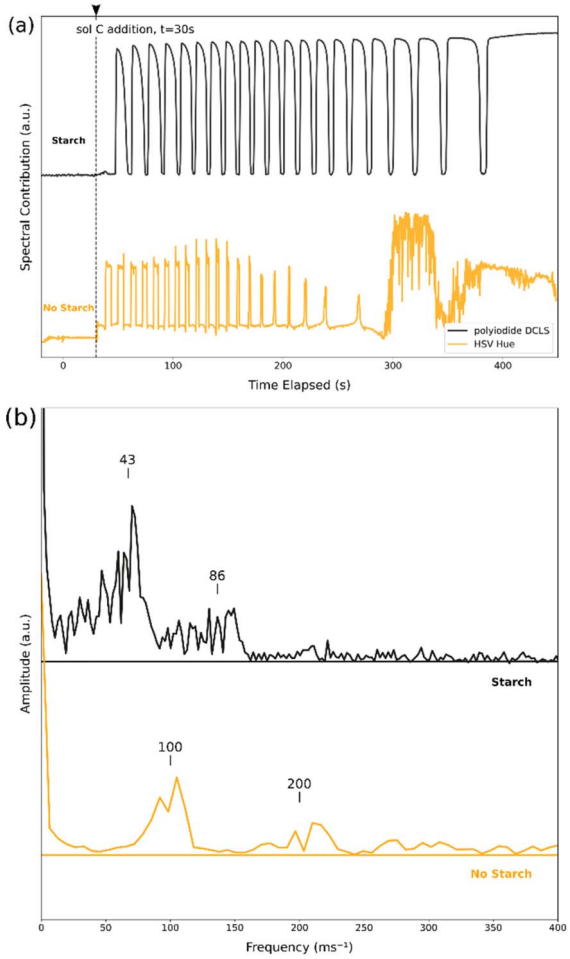

Fig. 6 Starch-dependent DCLS spectral contributions following the addition of solution C at (t = 30 s). (a) Time-resolved DCLS signals comparing systems with and without starch. In the presence of starch, sustained and regular oscillatory behaviour is observed, whereas the starch-free system exhibits less stable and more irregular transient dynamics. (b) Corresponding FFT spectra showing distinct low-frequency harmonic peaks for the starch-containing system and broader, higher-frequency features in the absence of starch.

The reaction transitions between yellow and clear phases at an accelerated rate, bypassing the characteristic blue-black complexation observed when starch is present (see Fig. 6a). This is noted by the slight change in relative luminosity, oscillating between 86% and 98%. The luminosity oscillation is not symmetrical, with the peak and trough luminosities increasing by approximately 0.5% each consecutive cycle of the reaction.

The yellow colouring of the solution indicates dissolved I_2, which has a minimum in the infrared region of its absorbance spectrum.[29] The Raman spectroscopic data reveals minimal chemical and physical changes because of this low absorbance of dissolved I_2 in the 785 nm region. At a critical point in the reaction cycle, the 877 cm^{-1} mode of H_2O_2 undergoes a marked decrease (Fig. S8). Simultaneously, the 980 and 802 cm^{-1} modes of manganese sulfate and IO_3^- respectively, decrease completely. This depletion coincides with a sharp increase in the 180 and 189 cm^{-1} Raman modes of solid iodine, indicating the abrupt precipitation of I_2. HSV analysis reveals a decline in luminosity and a shift in hue, indicating increased turbidity. As molecular iodine accumulates, a thin solid layer forms at the surface, scattering light and causing a luminosity increase as it reflects ambient light.

DCLS data were obtained by assigning the polyiodide spectra and the I_2 spectra for the non-starch and starch mixtures respectively (Fig. S8). Fig. 6 shows (a) a clear set of oscillations may be observed with the starch-present BR reaction, whereby no polyiodide oscillations took place with the starch-absent reaction in the DCLS and (b) FFT was applied to the HSV Hue values to obtain the oscillation frequency.

The starch-absent mixture displays an almost doubling in oscillation frequency compared with its starch-present mixture, parallel to the results of Csepei and Bolla.[30] Starch plays a crucial role in modulating the BR reaction, delaying molecular iodine from its reduction into I^-, and extends the oscillatory period. In its absence, free I_2 is more readily reduced, eliminating a stability and leading to a more rapid cycle of the reaction. The absence of starch also leads to the absence of polyiodide production. Starch's helical amylose structure traps I_2, creating a charge–transfer complex that shifts the equilibrium toward polyiodide formation, preventing the immediate reduction of I_2 back to I^-. Without starch, I_2 remains in free solution and is quickly reduced, minimising polyiodide formation. With starch, I_2 is retained longer, allowing more interaction with I^- ions to generate polyiodides.

Conclusion

Our study demonstrates the utility of real-time resonance Raman spectroscopy (785 nm) in probing the Briggs–Rauscher reaction, providing a chemically specific and temporally resolved alternative to conventional visual and electrochemical methods. In comparison with conventional BR reaction monitoring approaches, resonance Raman spectroscopy offers

several distinct advantages. Visual observation and camera-based HSV analysis provide colour-based proxies for iodine speciation but cannot resolve individual chemical species. Potentiometric iodide-selective electrodes offer real-time iodide quantification but are susceptible to fouling, require frequent recalibration, and do not respond selectively to a single species under the strongly oxidising and chemically complex conditions of the BR reaction. UV-visible spectroscopy provides molecular-level information but suffers from broad, overlapping absorbance bands and lower temporal resolution. By contrast, resonance Raman spectroscopy at 785 nm provides chemically specific, non-invasive, *in situ* identification and temporal tracking of discrete iodine species (I_5^-, I_3^-,and solid I_2) with sub-second time resolution, enabling direct correlation of spectral changes with visible colour dynamics. This approach reveals previously unobserved spectral transitions, highlighting the critical role of temperature, reagent concentrations, and the presence of starch in modulating the reaction dynamics. Specifically, increasing temperature from 5 °C to 43 °C progressively increases oscillation frequency, with loss of regular oscillatory character at the highest temperature tested; intermediate KIO_3 concentrations (94–200 mM) sustain well-defined oscillations, whereas sub-threshold (47 mM) or excessive concentrations suppress oscillatory behaviour. Furthermore, our results enhance the understanding of starch's role in the polyiodide–blue complex formation, demonstrating its direct influence on the stabilisation of polyiodide formation through its helical amylose structure. Starch actively stabilises polyiodide formation through its helical amylose structure, extending the oscillation period by approximately twofold relative to starch-free conditions, extending the oscillation period approximately twofold relative to starch-free conditions. The 785 nm excitation wavelength employed here extends prior Raman-based work at 632.8 nm (ref. 16) by reducing the Franck–Condon enhancement of the starch–iodine complex, thereby revealing spectral contributions in the 700–1000 cm^{-1} region and enabling simultaneous monitoring of reagent species (H_2O_2, IO_3^-, $MnSO_4$).

Author contributions

Conceptualization, R. G.; methodology, all authors; formal analysis, C. D. G., N. G., C. L.; investigation, all authors; resources, R. G., K. W., S. M.; data curation, C. D. G.; writing – original draft preparation, C. D. G.; writing – review and editing, all authors; supervision, R. G., K. W., S. M.; funding acquisition, K. W., R.G.; all authors have read and agreed to the published version of the manuscript.

Conflicts of interest

The authors declare no conflicts of interest.

Data availability

All BR reaction Raman data are available on GitHub (https://github.com/ClarkGray00/br_reaction).

Supplementary information (SI): additional experimental methods, Raman spectral assignments, pre-processing details, and supporting figures related to the real-time resonance Raman monitoring of the Briggs–Rauscher reaction. This comprises reference Raman spectra of individual reaction components and intermediates, time-resolved Raman and video correlation analyses, weighted moving average pre-processing procedures, and investigations into the effects of malonic acid, potassium iodate, hydrogen peroxide, temperature, and starch on oscillatory spectral behaviour using DCLS and FFT analyses. See DOI: https://doi.org/10.1039/d6ay00742b.

Acknowledgements

We thank James Blackhurst for building the optimisation translation stage necessary to create an optimised and reproducible Raman analysis system. C. G. is grateful to UK EPSRC for his Industrial CASE Studentship (EP/Y528766/1) with Renishaw.

References

1 I. R. Epstein and J. A. Pojman, *An introduction to nonlinear chemical dynamics: oscillations, waves, patterns, and chaos*, Oxford University Press, 1998.
2 K. R. Loos and A. C. Jones, Structure of triiodide ion in solution. Raman evidence for the existence of higher polyiodide species, *J. Phys. Chem.*, 1974, **78**(22), 2306–2307.
3 A. E. Johnson and A. B. Myers, Solvent Effects in the Raman Spectra of the Triiodide Ion: Observation of Dynamic Symmetry Breaking and Solvent Degrees of Freedom, *J. Phys. Chem.*, 1996, **100**(19), 7778–7788.
4 I. D. Yushina, B. A. Kolesov and E. V. Bartashevich, Raman spectroscopy study of new thia- and oxazinoquinolinium triodides, *New J. Chem.*, 2015, **39**(8), 6163–6170.
5 *kviht. Briggs-Rauscher reaction - Electrochemical measurement*, 2011, Available from: https://www.youtube.com/watch?v=SdKJwMVEhgU.
6 R. M. Noyes and S. D. Furrow, The oscillatory Briggs-Rauscher reaction. 3. A skeleton mechanism for oscillations, *J. Am. Chem. Soc.*, 1982, **104**(1), 45–48.
7 V. Vukojević, P. G. Sørensen and F. Hynne, Predictive Value of a Model of the Briggs−Rauscher Reaction Fitted to Quenching Experiments, *J. Phys. Chem.*, 1996, **100**(43), 17175–17185.
8 P. De Kepper and I. R. Epstein. Mechanistic Study of the Briggs-Rauscher Reaction, in, *Nonlinear phenomena in chemical dynamics*, Berlin, Heidelberg, Springer Berlin Heidelberg, 1981.
9 S. D. Furrow, A Modified Recipe and Variations for the Briggs–Rauscher Oscillating Reaction, *J. Chem. Educ.*, 2012, **89**(11), 1421–1424.
10 N. Muntean, *et al.*, Measurement of Hypoiodous Acid Concentration by a Novel Type Iodide Selective Electrode and a New Method To Prepare HOI. Monitoring HOI Levels in the Briggs–Rauscher Oscillatory Reaction, *J. Phys. Chem.*, 2012, **116**(25), 6630–6642.

11 W.-J. Xu, *et al.*, Fabrication of an iodide-selective electrode based on phthalocyaninatotitanium(IV) oxide and the selective determination of iodide in actual samples, *Anal. Bioanal. Chem.*, 2008, **392**(1), 297–303.
12 B. Rezaei, S. Meghdadi and V. Nafisi, Fast response and selective perchlorate polymeric membrane electrode based on bis(dibenzoylmethanato) nickel(II) complex as a neutral carrier, *Sensor. Actuator. B Chem.*, 2007, **121**(2), 600–605.
13 R. B. Beard, B. N. Hung and R. Schmukler, Biocompatibility considerations at stimulating electrode interfaces, *Ann. Biomed. Eng.*, 1992, **20**(3), 395–410.
14 M. J. Mahon and A. L. Smith, Kinetic Absorption Spectroscopy of the Briggs-Rauscher Oscillator, *J. Phys. Chem.*, 1985, **89**(7), 1215–1216.
15 A. Singhal, *et al.*, A Briggs-Rauscher Reaction-based Spectrometric Assay to Determine Antioxidant Content in Complex Matrices in Low Technology Environments, *Chimia*, 2021, **75**(1–2), 74–79.
16 B. Z. Chowdhry, *et al.*, Kinetic Resonance Raman Spectroscopy of the Briggs–Rauscher Oscillator, *ChemPhysChem*, 2002, **3**(5), 443–446.
17 Q. Jiang, Effect of lipids on starch determination through various methods, *Pakistan J. Agric. Sci.*, 2014, **51**, 749–755.
18 R. Muñiz, *et al.*, Two-Step Triethylamine-Based Synthesis of MgO Nanoparticles and Their Antibacterial Effect against Pathogenic Bacteria, *Nanomaterials*, 2021, **11**, 410.
19 Z. Xiao, R. Storms and A. Tsang, A quantitative starch-iodine method for measuring alpha-amylase and glucoamylase activities, *Anal. Biochem.*, 2006, **351**, 146–148.
20 T. S. Briggs and W. C. Rauscher, An oscillating iodine clock, *J. Chem. Educ.*, 1973, **50**(7), 496.
21 J. R. Durig, O. D. Bonner and W. H. Breazeale, Raman Studies of Iodic Acid and Sodium Iodate, *J. Phys. Chem.*, 1965, **69**(11), 3886–3892.
22 R. A. Cox, *et al.*, Resolution of Raman spectra of aqueous sulfuric acid mixtures using principal factor analysis, *Can. J. Chem.*, 1981, **59**(17), 2591–2598.
23 W. W. Rudolph and G. Irmer, Raman Spectroscopic Investigation of Speciation in MnSO4(aq), *J. Solut. Chem.*, 2014, **43**(3), 465–485.
24 V. Ananthanarayanan, Raman spectra of single crystals of dicarboxylic acids, *Proc. Indian Acad. Sci. Sect. A*, 1960, **51**(6), 328–335.
25 M. Almeida, *et al.*, Determination of amylose content in starch using Raman spectroscopy and multivariate calibration analysis, *Anal. Bioanal. Chem.*, 2010, **397**, 2693–2701.
26 M. L. Ramírez-Cedeño, *et al.*, Fiber Optic Coupled Raman Based Detection of Hazardous Liquids Concealed in Commercial Products, *Int. J. Spectrosc.*, 2012, **2012**(1), 463731.
27 A. Congeduti, M. Nardone and P. Postorino, Polarized Raman spectra of a single crystal of iodine, *Chem. Phys.*, 2000, **256**(1), 117–123.
28 S.-J. Zhang, *et al.*, Polyiodide Confinement by Starch Enables Shuttle-Free Zn–Iodine Batteries, *Adv. Mater.*, 2022, **34**(23), 2201716.
29 A. Mhatre, *et al.*, Functionalized glass fiber membrane for extraction of iodine species, *Separ. Sci. Technol.*, 2018, **54**, 1–9.
30 L. I. Csepei and C. Bolla, Is starch only a visual indicator for iodine in the Briggs-Rauscher oscillating reaction?, *Stud. Univ. Babes-Bolyai, Chem.*, 2015, **60**, 187–199.